Unified First-Principles Study of Gilbert Damping, Spin-Flip Diffusion, and Resistivity in Transition Metal Alloys

Anton A. Starikov,[1] Paul J. Kelly,[1] Arne Brataas,[2] Yaroslav Tserkovnyak,[3] and Gerrit E. W. Bauer[4]

[1]*Faculty of Science and Technology and* MESA$^+$ *Institute for Nanotechnology, University of Twente,*
P.O. Box 217, 7500 AE Enschede, The Netherlands
[2]*Department of Physics, Norwegian University of Science and Technology, N-7491 Trondheim, Norway*
[3]*Department of Physics and Astronomy, University of California, Los Angeles, California 90095, USA*
[4]*Kavli Institute of NanoScience, Delft University of Technology,*
Lorentzweg 1, 2628 CJ Delft, The Netherlands

Using a formulation of first-principles scattering theory that includes disorder and spin-orbit coupling on an equal footing, we calculate the resistivity ρ, spin-flip diffusion length l_{sf}, and Gilbert damping parameter α for $Ni_{1-x}Fe_x$ substitutional alloys as a function of x. For the technologically important $Ni_{80}Fe_{20}$ alloy, Permalloy, we calculate values of $\rho = 3.5 \pm 0.15$ $\mu\Omega$ cm, $l_{sf} = 5.5 \pm 0.3$ nm, and $\alpha = 0.0046 \pm 0.0001$ compared to experimental low-temperature values in the range 4.2–4.8 $\mu\Omega$ cm for ρ, 5.0–6.0 nm for l_{sf}, and 0.004–0.013 for α, indicating that the theoretical formalism captures the most important contributions to these parameters.

Introduction.—The drive to increase the density and speed of magnetic forms of data storage has focused attention on how magnetization changes in response to external fields and currents, on shorter length and time scales [1]. The dynamics of a magnetization **M** in an effective magnetic field $\mathbf{H}_{eff}$ is commonly described using the phenomenological Landau-Lifshitz-Gilbert equation

$$\frac{d\mathbf{M}}{dt} = -\gamma\mathbf{M} \times \mathbf{H}_{eff} + \mathbf{M} \times \left[\frac{\tilde{G}(\mathbf{M})}{\gamma M_s^2}\frac{d\mathbf{M}}{dt}\right], \quad (1)$$

where $M_s = |\mathbf{M}|$ is the saturation magnetization, $\tilde{G}(\mathbf{M})$ is the Gilbert damping parameter (that is, in general, a tensor), and the gyromagnetic ratio $\gamma = g\mu_B/\hbar$ is expressed in terms of the Bohr magneton μ_B and the Landé g factor, which is approximately 2 for itinerant ferromagnets. The *time* decay of a magnetization precession is frequently expressed in terms of the dimensionless parameter α given by the diagonal element of $\tilde{G}/\gamma M_s$ for an isotropic medium. If a nonequilibrium magnetization is generated in a disordered metal (for example, by injecting a current through an interface), its *spatial* decay is described by the diffusion equation

$$\frac{\partial^2 \Delta\mu}{\partial z^2} = \frac{\Delta\mu}{l_{sf}^2} \quad (2)$$

in terms of the spin accumulation $\Delta\mu$, the difference between the spin-dependent electrochemical potentials μ^σ for up and down spins, and the spin-flip diffusion length l_{sf} [2,3]. In spite of the great importance of α and l_{sf}, our understanding of the factors that contribute to their numerical values is, at best, sketchy. For clean ferromagnetic metals [4] and ordered alloys [5] however, recent progress has been made in calculating the Gilbert damping using the torque correlation model [6] and the relaxation time approximation in the framework of the Boltzmann equation. Estimating the relaxation time for particular materials and scattering mechanisms is, in general, a nontrivial task, and application of the torque correlation model to nonperiodic systems entails many additional complications and has not yet been demonstrated. Thus, the theoretical study of Gilbert damping or spin-flip scattering in disordered alloys and their calculation for particular materials with intrinsic disorder remain open questions.

Method.—In this Letter we calculate the resistivity ρ, spin-flip diffusion length l_{sf}, and Gilbert damping parameter α for substitutional $Ni_{1-x}Fe_x$ alloys within a single first-principles framework. To do so, we have extended a scattering formalism [7] based upon the local spin density approximation of density functional theory so that spin-orbit coupling (SOC) and chemical disorder are included on an equal footing. Relativistic effects are included by using the Pauli Hamiltonian.

For a disordered region of ferromagnetic (FM) alloy sandwiched between leads of nonmagnetic (NM) material, the scattering matrix S relates incoming and outgoing states in terms of reflection (r) and transmission (t) matrices at the Fermi energy. To calculate the scattering matrix, we use a "wave-function matching" scheme [7] implemented with a minimal basis of tight-binding linearized muffin-tin orbitals [8]. Atomic-sphere-approximation potentials [8] are calculated self-consistently using a surface Green's function method, also implemented [9] with tight-binding linearized muffin-tin orbitals. Charge and spin densities for binary alloy A and B sites are calculated using the coherent potential approximation (CPA) [10]

generalized to layer structures [9]. For the transmission matrix calculation, the resulting spherical potentials are assigned randomly to sites in large lateral supercells subject to maintenance of the appropriate concentration of the alloy [7]. Solving the transport problem using lateral supercells makes it possible to go beyond effective medium approximations such as the CPA. Because we are interested in the properties of bulk alloys, the leads can be chosen for convenience, and we use Cu leads with a single scattering state for each value of crystal momentum, $\mathbf{k}_{\parallel}$. The alloy lattice constants are determined using Vegard's law, and the lattice constants of the leads are made to match. Though NiFe is fcc only for the concentration range $0 \leq x \leq 0.6$, we use the fcc structure for all values of x.

For the self-consistent surface Green's function calculations (without SOC), the two-dimensional (2D) Brillouin zone (BZ) corresponding to the 1×1 interface unit cell was sampled with a 120×120 grid. Transport calculations including spin-orbit coupling were performed with a 32×32 2D BZ grid for a 5×5 lateral supercell, which is equivalent to a 160×160 grid in the 1×1 2D BZ. The thickness of the ferromagnetic layer ranged from 3 to 200 monolayers of fcc alloy; for the largest thicknesses, the scattering region contained more than 5000 atoms. For every thickness of ferromagnetic alloy, we averaged over a number of random disorder configurations; the sample to sample spread was small, and typically only five configurations were necessary.

Resistivity.—We calculate the electrical resistivity to illustrate our methodology. In the Landauer-Büttiker formalism, the conductance can be expressed in terms of the transmission matrix t as $G = (e^2/h)\mathrm{Tr}\{tt^{\dagger}\}$ [11,12]. The resistance of the complete system consisting of ideal leads sandwiching a layer of ferromagnetic alloy of thickness L is $R(L) = 1/G(L) = 1/G_{\mathrm{Sh}} + 2R_{\mathrm{if}} + R_b(L)$, where $G_{\mathrm{Sh}} = (2e^2/h)N$ is the Sharvin conductance of each lead with N conductance channels per spin, R_{if} is the interface resistance of a single NM|FM interface, and $R_b(L)$ is the bulk resistance of a ferromagnetic layer of thickness L [7,13]. When the ferromagnetic slab is sufficiently thick, Ohmic behavior is recovered whereby $R_b(L) \approx \rho L$, as shown in the inset to Fig. 1 for Permalloy (Py = Ni$_{80}$Fe$_{20}$), and the bulk resistivity ρ can be extracted from the slope of $R(L)$ [14]. For currents parallel and perpendicular to the magnetization direction, the resistivities are different and have to be calculated separately. The average resistivity is given by $\bar{\rho} = (\rho_{\parallel} + 2\rho_{\perp})/3$, and the anisotropic magnetoresistance ratio (AMR) is $(\rho_{\parallel} - \rho_{\perp})/\bar{\rho}$.

For Permalloy we find values of $\bar{\rho} = 3.5 \pm 0.15 \ \mu\Omega\,\mathrm{cm}$ and AMR $= 19 \pm 1\%$, compared to experimental low-temperature values in the range 4.2–4.8 $\mu\Omega\,\mathrm{cm}$ for $\bar{\rho}$ and 18% for AMR [15]. The resistivity calculated as a function of x is compared to low-temperature values from the literature [15] in Fig. 1. The plateau in the calculated values around the Py composition appears to be seen in the
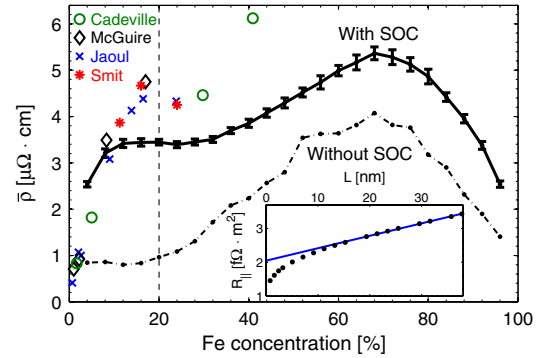

FIG. 1 (color online).   Calculated resistivity as a function of the concentration x for fcc Ni$_{1-x}$Fe$_x$ binary alloys with (solid line) and without (dashed-dotted line) SOC. Low-temperature experimental results are shown as symbols [15]. The composition Ni$_{80}$Fe$_{20}$ is indicated by a vertical dashed line. Inset: resistance of Cu|Ni$_{80}$Fe$_{20}$|Cu as a function of the thickness of the alloy layer. Dots indicate the calculated values averaged over five configurations, while the solid line is a linear fit.

experiments by Smit and Jaoul *et al.* [15]. The overall agreement with previous calculations is good [16]. In spite of the smallness of the SOC, the resistivity of Py is underestimated by more than a factor of 4 when it is omitted, underlining its importance for understanding transport properties.

Three sources of disorder which have not been taken into account here will increase the calculated values of ρ: short range potential fluctuations that go beyond the single site CPA, short range strain fluctuations reflecting the differing volumes of Fe and Ni, and spin disorder. These will be the subject of a later study.

Gilbert damping.—Recently, Brataas *et al.* showed that the energy loss due to Gilbert damping in an NM|FM|NM scattering configuration can be expressed in terms of the scattering matrix S [17]. Using the Landau-Lifshitz-Gilbert equation (1), the energy lost by the ferromagnetic slab is

$$\frac{dE}{dt} = \frac{d}{dt}(\mathbf{H}_{\mathrm{eff}} \cdot \mathbf{M}) = \mathbf{H}_{\mathrm{eff}} \cdot \frac{d\mathbf{M}}{dt} = \frac{1}{\gamma^2}\frac{d\mathbf{m}}{dt}\tilde{G}(\mathbf{M})\frac{d\mathbf{m}}{dt},$$ (3)

where $\mathbf{m} = \mathbf{M}/M_s$ is the unit vector of the magnetization direction for the macrospin mode. By equating this energy loss to the energy flow into the leads [18] associated with "spin pumping" [19],

$$I_E^{\mathrm{Pump}} = \frac{\hbar}{4\pi}\mathrm{Tr}\left\{\frac{dS}{dt}\frac{dS^{\dagger}}{dt}\right\} = \frac{\hbar}{4\pi}\mathrm{Tr}\left\{\frac{dS}{d\mathbf{m}}\frac{d\mathbf{m}}{dt}\frac{dS^{\dagger}}{d\mathbf{m}}\frac{d\mathbf{m}}{dt}\right\},$$ (4)

the elements of the tensor $\tilde{G}$ can be expressed as

$$\tilde{G}_{i,j}(\mathbf{m}) = \frac{\gamma^2\hbar}{4\pi}\mathrm{Re}\left\{\mathrm{Tr}\left[\frac{\partial S}{\partial m_i}\frac{\partial S^{\dagger}}{\partial m_j}\right]\right\}.$$ (5)

Physically, energy is transferred slowly from the spin degrees of freedom to the electronic orbital degrees of

freedom, from where it is rapidly lost to the phonon degrees of freedom. Our calculations focus on the role of elastic scattering in the rate-limiting first step.

Assuming that the Gilbert damping is isotropic for cubic substitutional alloys and allowing for the enhancement of the damping due to the FM|NM interfaces [19–21], the total damping in the system with a ferromagnetic slab of thickness L can be written $\tilde{G}(L) = \tilde{G}_{if} + \tilde{G}_b(L)$, where we express the bulk damping in terms of the dimensionless Gilbert damping parameter $\tilde{G}_b(L) = \alpha\gamma M_s(L) = \alpha\gamma\tilde{\mu}_s A L$, where $\tilde{\mu}_s$ is the magnetization density and A is the cross section. The results of calculations for $Ni_{80}Fe_{20}$ are shown in the inset to Fig. 2, where the derivatives of the scattering matrix in (5) were evaluated numerically by taking finite differences. The intercept at $L = 0$, $\tilde{G}_{if}$, allows us to extract the damping enhancement [20], but here we focus on the bulk properties and leave consideration of the material dependence of the interface enhancement for later study. The value of α determined from the slope of $\tilde{G}(L)/(\gamma\tilde{\mu}_s A)$ is 0.0046 ± 0.0001, which is at the lower end of the range of values 0.004–0.013 measured at room temperature for Py [21–23].

Figure 2 shows the Gilbert damping parameter as a function of x for $Ni_{1-x}Fe_x$ binary alloys in the fcc structure. From a large value for clean Ni, it decreases rapidly to a minimum at $x \sim 0.65$ and then grows again as the limit of clean fcc Fe is approached. Part of the decrease in α with increasing x can be explained by the increase in the magnetic moment per atom as we progress from Ni to Fe. The large values of α calculated in the dilute alloy limits can be understood in terms of conductivity-like enhancement at low temperatures [24], which has been explained in terms of intraband scattering [4,6]. The trend exhibited by the theoretical $\alpha(x)$ is seen to be reflected by experimental room-temperature results. In spite of a large spread in measured values, these seem to be systematically larger than the calculated values. Part of this discrepancy can be attributed to an increase in α with temperature [22,25].

Spin diffusion.—When an unpolarized current is injected from a normal metal into a ferromagnet, the polarization will return to the value characteristic of the bulk ferromagnet sufficiently far from the injection point, provided there are processes which allow spins to flip. Following Valet and Fert [3] and assuming there is no spin-flip scattering in the NM leads, we can express the fractional spin-current densities $p^{\uparrow(\downarrow)} = J^{\uparrow(\downarrow)}/J$ as a function of distance z from the interface as

$$p^{\uparrow(\downarrow)}(z) = \frac{1}{2} \pm \frac{\beta}{2}\left[1 - \frac{\exp(-z/l_{sf})r_{if}^*(\beta - \gamma + \gamma\delta)}{\beta(r_{if}^* + l_{sf}\delta\rho_F^*\tanh\delta)}\right],$$

(6)

where J is the total current through the device, $J^{\uparrow}$ and $J^{\downarrow}$ are the currents of majority and minority electrons, respectively, l_{sf} is the spin-diffusion length, $\rho_F^* = (\rho^{\downarrow} + \rho^{\uparrow})/4$ is the bulk resistivity, and β is the bulk spin asymmetry $(\rho^{\downarrow} - \rho^{\uparrow})/(\rho^{\downarrow} + \rho^{\uparrow})$. The interface resistance $r_{if}^* = (r_{if}^{\downarrow} + r_{if}^{\uparrow})/4$, the interface resistance asymmetry $\gamma = (r_{if}^{\downarrow} - r_{if}^{\uparrow})/(r_{if}^{\downarrow} + r_{if}^{\uparrow})$, and the interface spin-relaxation expressed through the spin-flip coefficient δ [26] must be taken into consideration, resulting in a finite polarization of the current injected into the ferromagnet. The corresponding expressions are plotted as solid lines in Fig. 3.

To calculate the spin-diffusion length we inject nonpolarized states from one NM lead and probe the transmission probability into different spin channels in the other NM lead for different thicknesses of the ferromagnet. Figure 3 shows that the calculated values can be fitted using expressions (6) if we assume that $J^{\sigma}/J = G^{\sigma}/G$, yielding values of the spin-flip diffusion length $l_{sf} = 5.5 \pm 0.3$ nm and bulk asymmetry parameter $\beta = 0.678 \pm 0.003$ for $Ni_{80}Fe_{20}$ alloy, compared to experimentally estimated values of 0.7 ± 0.1 for β and in the range 5.0–6.0 nm for l_{sf} [27].

l_{sf} and β are shown as a function of the concentration x in Fig. 4. The convex behavior of β is dominated by and
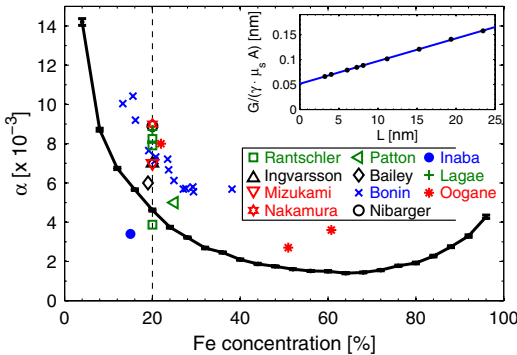

FIG. 2 (color online).   Calculated zero-temperature (solid line) and experimental room-temperature (symbols) values of the Gilbert damping parameter as a function of the concentration x for fcc $Ni_{1-x}Fe_x$ binary alloys [21–23]. Inset: total damping of $Cu|Ni_{80}Fe_{20}|Cu$ as a function of the thickness of the alloy layer. Dots indicate the calculated values averaged over five configurations, while the solid line is a linear fit.
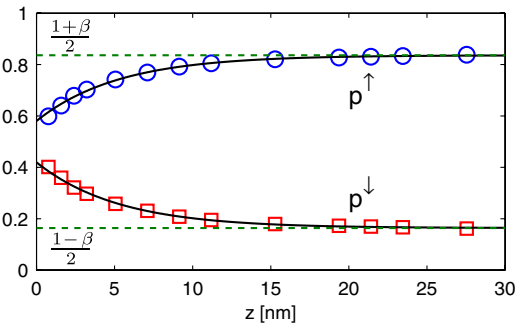

FIG. 3 (color online).   Fractional spin-current densities for electrons injected at $z = 0$ from Cu into $Ni_{80}Fe_{20}$ alloy. Symbols indicate calculated values, while the solid lines are fits to Eq. (6).
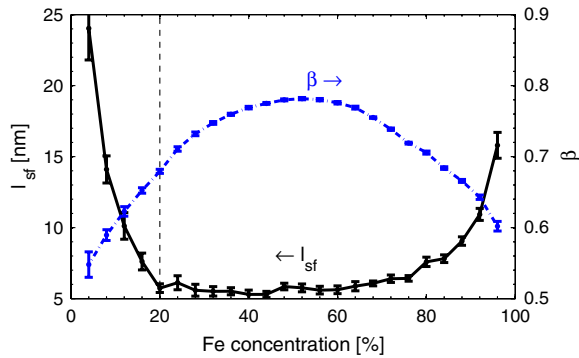
FIG. 4 (color online). Spin-diffusion length (solid line) and polarization β as a function of the concentration x for $Ni_{1-x}Fe_x$ binary alloys.

tracks the large minority spin resistivity $\rho^{\downarrow}$ whose origin is the large mismatch of the Ni and Fe minority spin band structures that leads to a $\sim x(1-x)$ concentration dependence of $\rho^{\downarrow}(x)$ [16]. The majority spin band structures match well, so $\rho^{\uparrow}$ is much smaller and changes relatively weakly as a function of x. The increase of l_{sf} in the clean metal limits corresponds to the increase of the electron momentum and spin-flip scattering times in the limit of weak disorder.

In summary, we have developed a unified density functional theory-based scattering theoretical approach for calculating transport parameters of concentrated alloys that depend strongly on spin-orbit coupling and disorder and have illustrated it with an application to NiFe alloys. Where comparison with experiment can be made, the agreement is remarkably good, offering the prospect of gaining insight into the properties of a host of complex but technologically important magnetic materials.

[1] See the collection of articles in *Ultrathin Magnetic Structures I–IV*, edited by J. A. C. Bland and B. Heinrich (Springer-Verlag, Berlin, 1994).

[2] P. C. van Son, H. van Kempen, and P. Wyder, Phys. Rev. Lett. **58**, 2271 (1987); **60**, 378 (1988).

[3] T. Valet and A. Fert, Phys. Rev. B **48**, 7099 (1993).

[4] K. Gilmore, Y. U. Idzerda, and M. D. Stiles, Phys. Rev. Lett. **99**, 027204 (2007); J. Appl. Phys. **103**, 07D303 (2008); V. Kamberský, Phys. Rev. B **76**, 134416 (2007).

[5] C. Liu et al., Appl. Phys. Lett. **95**, 022509 (2009).

[6] V. Kamberský, Czech. J. Phys. **26**, 1366 (1976).

[7] K. Xia et al., Phys. Rev. B **63**, 064407 (2001); **73**, 064420 (2006).

[8] O. K. Andersen, Z. Pawlowska, and O. Jepsen, Phys. Rev. B **34**, 5253 (1986); O. K. Andersen, *ibid.* **12**, 3060 (1975).

[9] I. Turek et al., *Electronic Structure of Disordered Alloys, Surfaces and Interfaces* (Kluwer, Boston-London-Dordrecht, 1997).

[10] P. Soven, Phys. Rev. **156**, 809 (1967).

[11] M. Büttiker et al., Phys. Rev. B **31**, 6207 (1985).

[12] S. Datta, *Electronic Transport in Mesoscopic Systems* (Cambridge University Press, Cambridge, England, 1995).

[13] K. M. Schep et al., Phys. Rev. B **56**, 10805 (1997).

[14] The nonlinearity of the resistance for $L \lesssim 20$ in the inset to Fig. 1 has nothing to do with spin-orbit coupling. It results when spin-dependent resistances of the form $R^{\sigma}(L) = 2/G_{Sh} + 2R_{if}^{\sigma} + \rho^{\sigma} L$ are added in parallel in the two-current series-resistor model; the total resistance only becomes linear for values of L so large that the bulk resistances $\rho^{\sigma} L$ are much larger than the interface and Sharvin terms.

[15] J. Smit, Physica (Amsterdam) **17**, 612 (1951); T. R. McGuire and R. I. Potter, IEEE Trans. Magn. **11**, 1018 (1975); O. Jaoul, I. A. Campbell, and A. Fert, J. Magn. Magn. Mater. **5**, 23 (1977); M. C. Cadeville and B. Loegel, J. Phys. F **3**, L115 (1973).

[16] J. Banhart and H. Ebert, Europhys. Lett. **32**, 517 (1995); J. Banhart, H. Ebert, and A. Vernes, Phys. Rev. B **56**, 10165 (1997).

[17] A. Brataas, Y. Tserkovnyak, and G. E. W. Bauer, Phys. Rev. Lett. **101**, 037207 (2008).

[18] J. E. Avron et al., Phys. Rev. Lett. **87**, 236601 (2001); M. Moskalets and M. Büttiker, Phys. Rev. B **66**, 035306 (2002); **66**, 205320 (2002).

[19] Y. Tserkovnyak, A. Brataas, and G. E. W. Bauer, Phys. Rev. Lett. **88**, 117601 (2002); Phys. Rev. B **66**, 224403 (2002).

[20] M. Zwierzycki et al., Phys. Rev. B **71**, 064420 (2005).

[21] S. Mizukami, Y. Ando, and T. Miyazaki, J. Magn. Magn. Mater. **226–230**, 1640 (2001); Jpn. J. Appl. Phys. **40**, 580 (2001).

[22] W. Bailey et al., IEEE Trans. Magn. **37**, 1749 (2001).

[23] C. E. Patton, Z. Frait, and C. H. Wilts, J. Appl. Phys. **46**, 5002 (1975); S. Ingvarsson et al., Appl. Phys. Lett. **85**, 4995 (2004); H. Nakamura et al., Jpn. J. Appl. Phys. **43**, L787 (2004); J. O. Rantschler et al., IEEE Trans. Magn. **41**, 3523 (2005); R. Bonin et al., J. Appl. Phys. **98**, 123904 (2005); L. Lagae et al., J. Magn. Magn. Mater. **286**, 291 (2005); J. P. Nibarger et al., Appl. Phys. Lett. **83**, 93 (2003); N. Inaba et al., IEEE Trans. Magn. **42**, 2372 (2006); M. Oogane et al., Jpn. J. Appl. Phys. **45**, 3889 (2006).

[24] S. M. Bhagat and P. Lubitz, Phys. Rev. B **10**, 179 (1974); B. Heinrich, D. J. Meredith, and J. F. Cochran, J. Appl. Phys. **50**, 7726 (1979).

[25] D. Bastian and E. Biller, Phys. Status Solidi A **35**, 113 (1976).

[26] W. Park et al., Phys. Rev. B **62**, 1178 (2000).

[27] J. Bass and W. P. Pratt, Jr., J. Magn. Magn. Mater. **200**, 274 (1999); J. Phys. Condens. Matter **19**, 183201 (2007).